Sea surface temperatures of the western Arabian Sea during the last deglaciation

M. H. Saher,[1] S. J. A. Jung,[1] H. Elderfield,[2] M. J. Greaves,[2] and D. Kroon[1]

Received 15 March 2006; revised 1 November 2006; accepted 12 December 2006; published 4 May 2007.

[1] In this study we present a sea surface temperature (SST) record from the western Arabian Sea for the last 20,000 years. We produced centennial-scale $\delta^{18}O$ and Mg/Ca SST time series of core NIOP929 with focus on the glacial-interglacial transition. The western Arabian Sea is influenced by the seasonal NE and SW monsoon wind systems. Lowest SSTs occur during the SW monsoon season because of upwelling of cold water, and highest SSTs can be found in the low-productivity intermonsoon season. The Mg/Ca-based temperature record reflects the integrated SST of the SW and NE monsoon seasons. The results show a glacial-interglacial SST difference of ~2°C, which is corroborated by findings from other Arabian Sea cores. At 19 ka B.P. a yet undescribed warm event of several hundred years duration is found, which is also reflected in the $\delta^{18}O$ record. A second centennial-scale high SST/low $\delta^{18}O$ event is observed at 17 ka B.P. This event forms the onset of the stepwise yet persistent trend toward Holocene temperatures. Highest Mg/Ca-derived SSTs in the NIOP929 record occurred between 13 and 10 ka B.P. Interglacial SST is ~24°C, indicating influence of upwelling. The onset of Arabian Sea warming occurs when the North Atlantic is experiencing minimum temperatures. The rapid temperature variations at 19, 17, and 13 ka B.P. are difficult to explain with monsoon changes alone and are most likely also linked to regional hydrographic changes, such as trade wind induced variations in warm water advection.

Citation: Saher, M. H., S. J. A. Jung, H. Elderfield, M. J. Greaves, and D. Kroon (2007), Sea surface temperatures of the western Arabian Sea during the last deglaciation, *Paleoceanography*, *22*, PA2208, doi:10.1029/2006PA001292.

1. Introduction

[2] Monsoon-dominated climate systems are the most dynamic coupled atmosphere-ocean-continent systems on Earth [*Webster et al.*, 1998, and references therein]. The Arabian Sea is affected by the west Asian monsoon system [*Brock et al.*, 1992; *Prell and Curry*, 1981; *Rixen et al.*, 1996; *Shetye et al.*, 1994], which controls environmental conditions in large parts of the area. The seasonal change from the summer SW monsoon to the winter NE monsoon affects surface ocean properties and largely controls the environmental conditions over the Asian subcontinent. In the monsoon-induced upwelling areas in the western Arabian Sea, cool sea surface temperatures (SSTs) prevail during summer, reflecting the subsurface origin of these waters. During winter, upwelling ceases and sea surface temperatures are higher. The highest temperatures occur in the intermonsoon seasons; these, however, are only marginally documented in the proxy records used since foraminiferal productivity is low in these seasons [*Conan and Brummer*, 2000; *Curry et al.*, 1992].

[3] Several authors have studied the glacial-interglacial SST history of the Arabian Sea [*Emeis et al.*, 1995; *Rostek et al.*, 1997; *ten Haven and Kroon*, 1991], concluding that the SST history of the basin is primarily dictated by the global glacial-interglacial SST signal, with low glacial and high interglacial SST, respectively. Similarly, the history of the Indian monsoon system was mainly dominated by glacial-interglacial cycles [e.g., *Bigg and Jiang*, 1993; *Prell et al.*, 1992]. During glacial periods, snow cover on the Tibetan Plateau possibly increased [*Benn and Owen*, 1998], and SSTs in the South Indian Ocean were lower [*Sonzogni et al.*, 1998]. This resulted in reduced SW monsoon strength [*Anderson and Prell*, 1993; *Prell and Campo*, 1986], whereas the NE monsoon was intensified [*Duplessy*, 1982; *Fontugne and Duplessy*, 1986; *Prell and Campo*, 1986].

[4] The Arabian Sea has received increasing attention in the context of the current debate on the hemispheric phasing of millennial- to centennial-scale climate changes [*Alley et al.*, 2002; *Bard et al.*, 1997; *Blunier and Brook*, 2001; *Blunier et al.*, 1998; *Broecker*, 1998]. On the basis of comparably low resolution records a number of authors concluded that the climate pattern changed in phase with the northern Atlantic Ocean [*Altabet et al.*, 1995; *Leuschner and Sirocko*, 2000; *Reichart et al.*, 1998; *Schulte and Müller*, 2001; *Schulz et al.*, 1998]. *Schulz et al.* [1998] confirmed this conclusion from a millennial-scale palaeoproductivity record by demonstrating a parallel change in the strength of the oxygen minimum zone in the Arabian Sea and temperatures over Greenland. A comparable relationship was found in the palaeoproductivity signal of sediments off Somalia [*Ivanochko et al.*, 2005; *Jung et al.*, 2002].

[1] Institute of Earth Sciences, Vrije Universiteit Amsterdam, Amsterdam, Netherlands.
[2] Department of Earth Sciences, University of Cambridge, Cambridge, UK.

0883-8305/07/2006PA001292$12.00

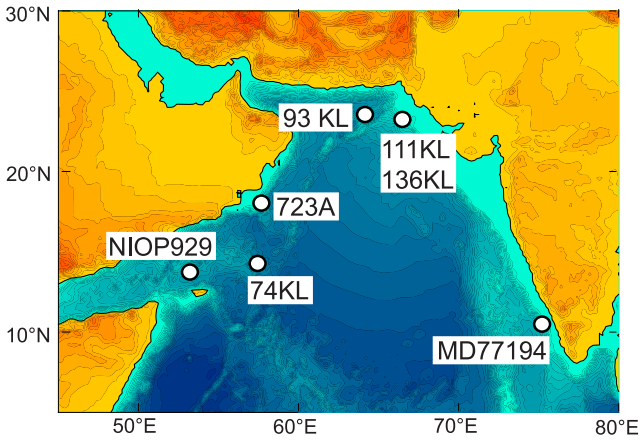

Figure 1. Location of cores NIOP929 [*Ivanova*, 1999], 74KL [*Sirocko et al.*, 1993], 93KL, 111KL, 136KL [*Schulz et al.*, 1998], and MD77194 [*Cayre and Bard*, 1999] and ODP Hole 723A [*Anderson and Prell*, 1993].

[5] Here we present a combined δ^{18}O-Mg/Ca time series of sediment core NIOP929 with a centennial-scale time resolution. We aim to relate SST changes in core NIOP929 to regional temperature trends and monsoonal activity by comparing them to other Arabian Sea SST records. This will answer whether the synchronicity of low productivity in the Arabian Sea with North Atlantic cold periods is also seen in the area of core NIOP929. Subsequently, we can assess how possible productivity minima relate to SST and how the observed temperature patterns constrain monsoon intensity in these periods.

2. Modern Monsoonal Change in the Arabian Sea

[6] Core NIOP929, in some studies referred to as TY93-929P2 [*Rostek et al.*, 1997], was taken as part of the Netherlands Indian Ocean Programme [*van Hinte et al.*, 1995]. The core was retrieved from the western Arabian Sea (Figure 1) (13°42′21″N, 53°14′76″E) at 2490 m water depth. Currently, the site of core NIOP929 is strongly affected by the seasonal change in monsoonal airflow. Differential heating of the ocean waters and continental landmasses results in a seasonally reversing atmospheric pressure gradient. In boreal summer the pressure low over Tibet causes the intertropical convergence zone (ITCZ) to shift north and induces the strong southwest monsoon. Ekman transport caused by these winds induces upwelling of cold water, thereby lowering the sea surface temperature. In winter the ITCZ shifts south, and the weaker northeasterly winds of the winter monsoon allow the surface waters of the Arabian Sea to become stratified and heat up relative to the summer. We aimed to understand the temperature history at the centennial to millennial scale. A complex SST history is anticipated as variations in both monsoon wind systems must have influenced SST. Northern Hemisphere cold periods, for instance, could, on the one hand, result in cold NE monsoon winds cooling the water surface and, on the other hand, result in reduced SW monsoon strength with associated reduced upwelling and therefore high SSTs. In addition, other factors may have been involved in the SST evolution, such as regional SST variations induced by oceanic currents as a result of trade wind variability.

3. Age Model

[7] The age model of core NIOP929 is based on nine accelerator mass spectrometry (AMS) ^{14}C dates (Table 1 and Figure 2). One AMS ^{14}C date was given by *Ivanova* [1999], and eight new AMS ^{14}C dates are based on the planktonic foraminifera species *Globorotalia menardii*. In most cases we used tests from the size fraction >355 μm, from one up to three consecutive samples. For one date, additional specimens from the size fraction 250-355 μm were used. For the sample at 21 cm depth this procedure did not provide enough material for AMS ^{14}C analysis, and specimens of other planktonic foraminifera species (*Globigerina bulloides, Globigerinoides ruber,* and *Neogloboquadrina dutertrei*) were added (Table 1). The AMS measurements were performed in the R. J. van de Graaff laboratory in Utrecht. The ^{14}C ages were calibrated to calendar ages using the program Calib5 (version 5.0 [*Stuiver and Reimer*, 1993]), taking into account a reservoir age of 600 years [*Southon et al.*, 2002; *Staubwasser et al.*, 2002; *von Rad et al.*, 1999].

[8] The age/depth relationship using the age control points in Figure 2 shows one reversal, at 166.5 cm depth. At this depth the abundance of *G. menardii* is low (Figure 3). The

Table 1. The ^{14}C Ages of Core NIOP929

Depth,[a] cm bsf	Number of Lumped Samples	^{14}C Age	Error (1σ)	Species	Size Fraction	Calendar Age, years B.P.
21.0–22.5	3	1952	42	mixed plankton[b]	250 μm+	1292
50.5–51.5	2	5550	46	*G. menardii*	250 μm+	5699
76.5–77.0	1	8560	50	*G. menardii*	355 μm+	8929
82.0–82.5	1	9249	51	*G. menardii*	355 μm+	9737
110.5–111.0	1	10,708[c]	52	*G. menardii*	355 μm+	11,651
125.0–125.5	1	12,270	57	*G. menardii*	355 μm+	13,508
166.5–167.0	1	11,813[c]	57	*G. menardii*	355 μm+	13,101
180.0–180.5	1	15,620	70	mixed planktonc[b]	250 μm+	18,313
210.5–211.0	1	17,380	85	*G. menardii*	355 μm+	19,920

[a]Below seafloor.
[b]Mixed plankton: *G. menardii, G. bulloides, G. ruber,* and *N. dutertrei*.
[c]These ^{14}C Ages were not used in the construction of the age model. See text for explanation.

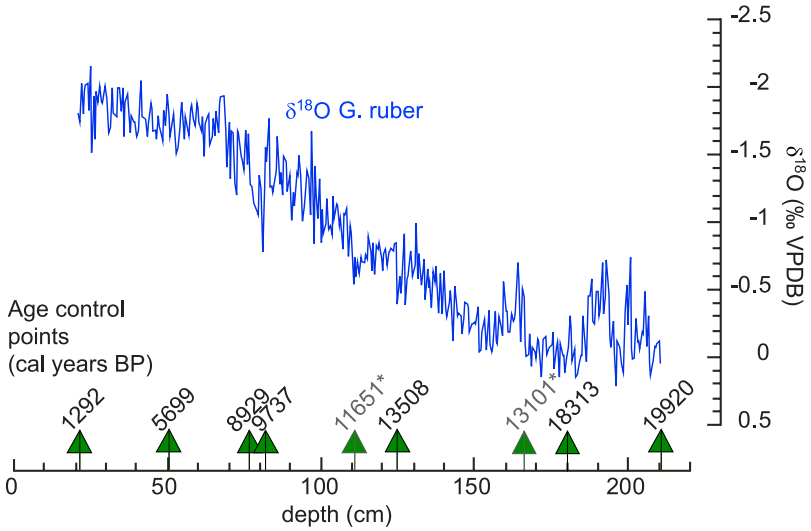

Figure 2. Core NIOP929 $\delta^{18}O$ record of the planktonic foraminifera species *G. ruber* plotted against depth. The age points (calibrated to calendar age) on which the age model was based are also depicted. This age model was constructed by linearly interpolating between these tie points. The asterisks indicate age points that were not used in the age model; see text for discussion.

^{14}C age of this sample corresponds roughly with that of the adjacent *G. menardii* abundance peak (at 13.5 ka B.P.). We therefore assume that the specimens of *G. menardii* present in this sample were bioturbated down from this level, leading to an underestimation of the age of this sample. A similarly low abundance of *G. menardii* occurred at 110.5 cm depth. Both dates were not incorporated into the age model (Figures 2 and 3).

3.1. Material and Methods

[9] The 16.15 m long core NIOP929 covers the last 240 ka, having an average sedimentation rate of 15 cm/ka [*Ivanova*, 1999]. The coring location was on a local high, minimizing potential effects on the sediment record by lateral sediment advection/redeposition. Previous workers sampled the core at a 10 and 5 cm sample resolution to reveal the long-term evolution of $\delta^{18}O$ and $\delta^{13}C$ in several species of planktonic foraminifera (*G. bulloides*, *G. ruber,* and *N. dutertrei*), faunal assemblages C_{org}, fragmentation index [*Ivanova*, 1999], and $U^{k'}_{37}$ [*Rostek et al.*, 1997]. For this study, sediment sections covering the last 20 ka, i.e., the upper 210 cm of core NIOP929, were continuously sampled at 0.5 cm resolution (Figure 2). The sampled interval has an average sedimentation rate of ~10 cm/ka. Hence the 0.5 cm sampling results in an average time resolution of ~50 years.

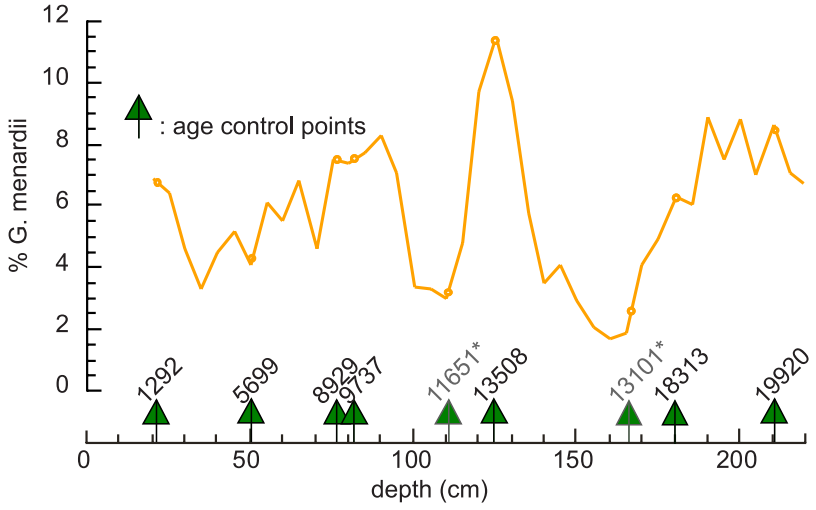

Figure 3. Percentages of *G. menardii* against depth in core NIOP929. Notice the low values of *G. menardii* at 110.5 and 166.5 cm depth. The anomalously young age of the sample at 166.5 cm might be due to contamination from specimens from a shallower depth. The age of the sample at 110.5 cm is not anomalous, yet the low abundance of *G. menardii* at that level and the high abundances at the adjacent level are a cause for suspicion.

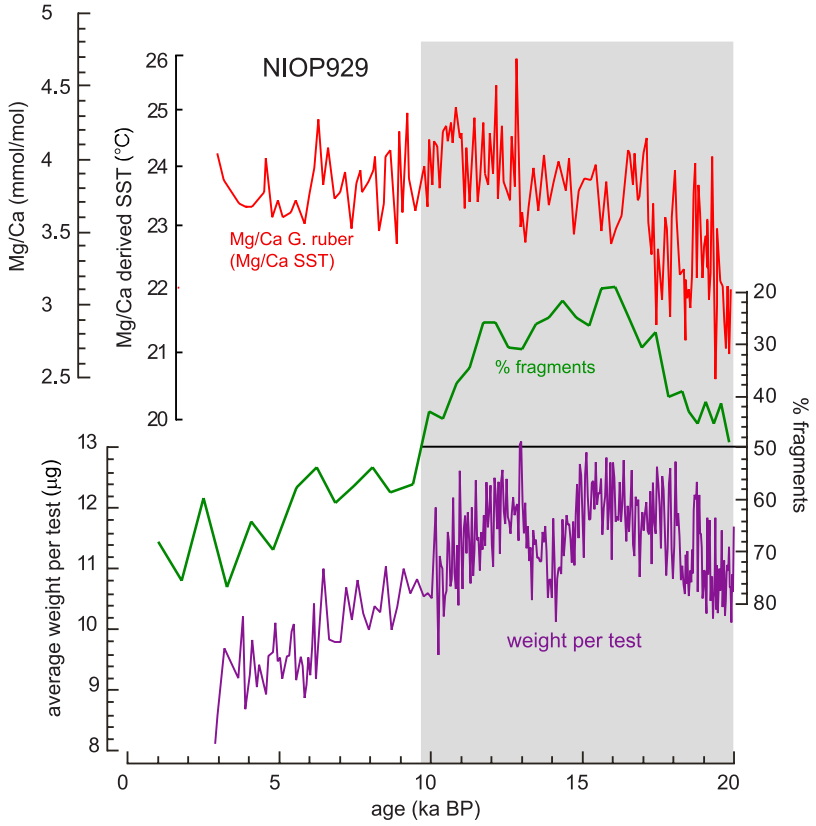

Figure 4. Mg/Ca (SST) record of core NIOP929 is plotted together with the percentage of fragments [*Ivanova*, 1999] and weight per test. The Mg/Ca to temperature conversion was performed with the equation by *Anand et al.* [2003]. The grey area indicates the part of the core in which the percentage of fragments stays below 50%. The remaining part of the plot might be affected by dissolution, which might cause an offset in calculated SST of ~1°C.

[10] The sample slices were freeze-dried and wet-sieved over a 63 μm sieve. Fifty tests of *G. ruber* were picked from the 250–355 μm fraction. Twenty specimens of *G. ruber* were used for Mg/Ca measurement, and 30 were used for stable isotope measurements. Occasionally, samples did not contain 50 specimens of *G. ruber*, and isotopic measurements were performed on less than 30 (down to 10) specimens. For stable isotope measurements the tests were crushed, and ~30 μg were taken from the homogenized sample and measured on a Finnigan MAT252 equipped with a Kiel device. The internal error (1σ) of the mass spectrometer is 0.08‰ for $\delta^{18}O$ and 0.05‰ for $\delta^{13}C$. All isotope measurements were performed at the Institute of Earth Sciences at the Vrije Universiteit Amsterdam.

[11] The Mg/Ca measurements were mostly performed at 1 cm sample spacing. Occasionally, analyses from variably spaced samples (sample spacing between 0.5 and 3 cm) were used. For the Mg/Ca measurements, 20 tests of *G. ruber* were gently crushed between glass plates and subjected to a cleaning process designed to remove clay and organic matter [*Barker et al.*, 2003]. In addition, the samples were centrifuged for 5 min at 5000 rpm after dissolution in 350 μL HNO_3 in order to settle any remaining small-silicate particles. After centrifuging, the samples were transferred to a clean vial, leaving 50 μL containing any remaining residue behind. The measurements were performed at the Department of Earth Sciences at Cambridge University on a Varian Vista AX [*de Villiers et al.*, 2002]. The effectiveness of cleaning was monitored by measuring Al/Ca, Fe/Ca, Mn/Ca, and Ti/Ca simultaneously with Mg/Ca. Mg/Ca ratios were converted to temperature estimates using the equation by *Anand et al.* [2003].

3.2. Evaluation of the Mg/Ca Measurements

[12] Mg/Ca ratios in foraminiferal tests can be affected by dissolution [*Brown and Elderfield*, 1996; *Elderfield and Ganssen*, 2000; *Rosenthal and Lohmann*, 2002; *Rosenthal et al.*, 2000]. The robustness of the temperature reconstruction using the core NIOP929 Mg/Ca data was evaluated using two dissolution proxies (Figure 4), namely, average shell weight and fragmentation. To obtain a narrow size range for the average shell weight, the 250–355 μm size fraction of the *G. ruber* samples was sieved over a 300 μm sieve. The 250–300 μm fraction was counted and weighed on a Sartorius microbalance (micro M 3 P) with a precision of $\leq$1 μg. The resultant test weight represents an average value for a population of, on average, 34 tests. After weighing, the 250–300 μm and 300–355 μm fractions were recombined.

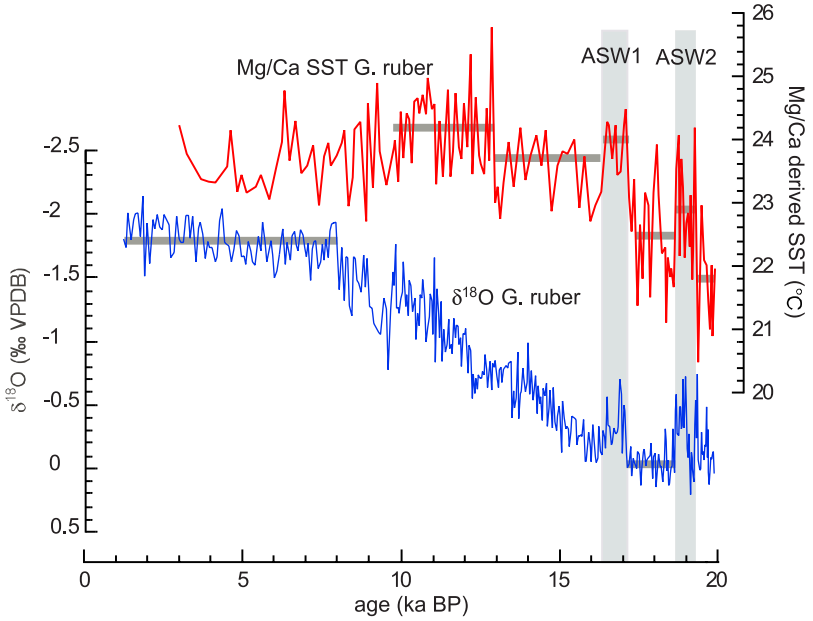

Figure 5. Core NIOP929 δ^{18}O record and Mg/Ca-based temperature estimate of *G. ruber*. The grey lines superimposed on the curves give average values over the time interval they cover. Notice that the part of the Mg/Ca SST record younger than 9.7 ka B.P. (see Figure 4) was not used in calculations of the average. The grey vertical bars indicate the Arabian Sea warm events 1 and 2 (ASW1 and ASW2).

[13] Low-resolution foraminiferal fragmentation data were available from *Ivanova* [1999] (Figure 4). Fragmentation depends on various factors [*Barker and Elderfield*, 2002; *Bijma et al.*, 2002; *Broecker and Clark* 2001a, 2001b; *Conan et al.*, 2002; *Lohmann*, 1995] yet can be used as an indication of dissolution [*de Villiers*, 2003]. The shell weight and fragmentation records show a general similarity. We took the conspicuous shift toward higher percentages of fragments at 9.7 ka B.P., corroborated by the concomitant trend toward lower shell weights with decreasing depth, as indicative of increased dissolution (Figure 4). Mg/Ca-based SST estimates from the interval with a higher percentage of fragments are considered less reliable. Application of the correction equation of *Rosenthal and Lohmann* [2002] suggests that the possible dissolution-related error in the upper 10,000 years of the record ranges from 0.4° to 2.3°C, with an average of 1.3°C.

4. Results

4.1. The δ^{18}O Record

[14] The δ^{18}O record of core NIOP929 (Figure 5) covers the time interval 20 ka B.P. (Last Glacial Maximum (LGM)) [*Mix et al.*, 2001] to 1 ka B.P. (late Holocene) on a decadal scale. The total range of δ^{18}O values is ~0.2 (LGM) to ~−2.2‰ (late Holocene), with average glacial and interglacial values of 0.0 and −1.8‰, respectively. The record shows a highly variable LGM period followed by the start of the deglaciation at 17.1 ka B.P. The δ^{18}O values steadily decrease to 8.0 ka B.P., apart from a reversal in the trend between 13.4 and 12.2 ka B.P. From 8.0 ka B.P. onward the record expresses a gentle trend toward lower values.

[15] The long-term trends in the oxygen isotope record are superimposed by centennial-scale low δ^{18}O events and rapid shifts (Figure 5). A prominent δ^{18}O minimum, with average amplitude of ~−0.4‰, occurs around 18.9 ka B.P. on a presumably fully glacial background. It is preceded by a short (100 years) negative peak with similar amplitude, centered around 19.4 ka B.P. A second 600 year long δ^{18}O minimum spike, with average amplitude of ~−0.3‰, is centered around 16.8 ka B.P. After the end of this low δ^{18}O period, δ^{18}O decreases gradually. The decrease is punctuated by a brief positive excursion centered around 13.8 ka B.P. Successively, the δ^{18}O values gradually increase by ~+0.2‰ followed by a sharp shift of −0.4‰ at 12.2 ka B.P. After the deglaciation, a sharp positive excursion occurs at 9.5 ka B.P. (Figure 5). This peak has a duration of ~700 years with the initial +1‰ shift occurring in just over 200 years.

[16] We compare our δ^{18}O record with two previously published Arabian Sea δ^{18}O records of *G. ruber*, namely, those of cores SO93-74KL (14°19′26″N, 57°20′82″E, water depth 3212 m) [*Sirocko et al.*, 1993] and SO90-93KL (23°35′30″N, 64°13′01″E, water depth 1802 m) [*Schulz et al.*, 1998], which are hereafter referred to as 74KL and 93KL, respectively. This comparison allows us to asses whether the patterns observed in our record reflect local or regional climate variation and provides a check for our age model. As can be seen in Figure 6 the patterns in the three records are largely comparable. The similarity of our record to 74KL is greater than to 93KL, which is as expected because of the greater proximity to 74KL. The two prominent periods of low δ^{18}O at 19.4 and 16.8 ka B.P. can be

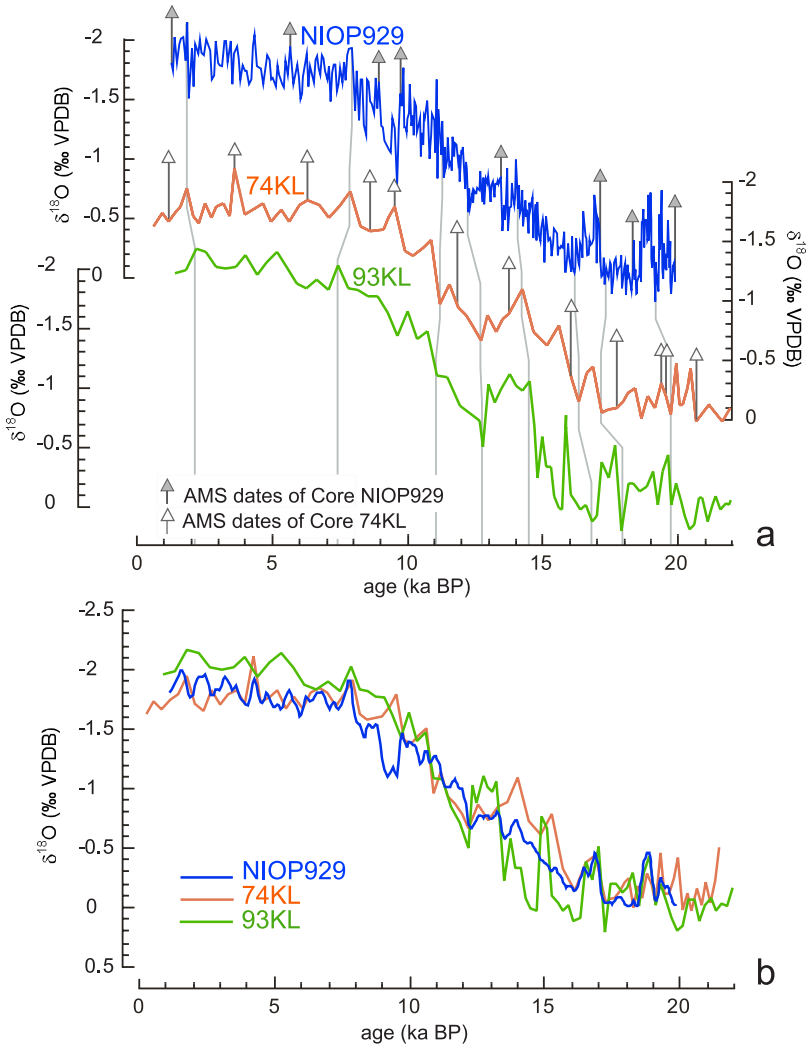

Figure 6. (a) The δ^{18}O records (*G. ruber*) from the Arabian Sea. The data of core 74KL were reproduced from *Sirocko et al.* [1993]. The data of core 93KL were given by *Schulz et al.* [1998]. All data have been plotted on their individual age scales. The grey lines indicate correlation tie points. The white-headed arrows are ^{14}C AMS dates of core 74KL, and the grey-headed arrows are ^{14}C AMS dates of core NIOP929. (b) The δ^{18}O records (*G. ruber*) of cores NIOP929, 74KL [*Sirocko et al.*, 1993], and 93KL [*Schulz et al.*, 1998]. The δ^{18}O records of 74KL and 93KL are tuned to the δ^{18}O record of core NIOP929, according to the tie points in Figure 6a. For improved visibility the record of core NIOP929 was first filtered to exclude frequencies higher than 1/500 years.

traced through all three records, indicating that these are most likely a regional feature.

4.2. Mg/Ca Temperature Reconstruction

[17] The Mg/Ca-based temperature record of core NIOP929 displays a stepwise evolution across termination I (Figure 5). The late glacial period between 20 and 17 ka B.P. displays high variability with a pronounced warming from 19.3 to 18.7 ka B.P. At 17 ka B.P., SST rapidly rose to 24°C and subsequently decreased to 23.5°C around 16 ka B.P. A second stepwise temperature increase to >24°C occurred at 12.9 ka B.P. Superimposed on these long-term changes, the record is highly variable. The low δ^{18}O event around 18.9 ka B.P. is concomitant with a warm event with average amplitude of ~1°C (maximum change 3.5°C) that precedes the δ^{18}O event by about 300 years. The δ^{18}O minimum around 16.8 ka B.P. is synchronous with a discrete warm period of ~1.5°C higher than background values. To simplify reference to this warm period, we will refer to it as Arabian Sea warm event I (ASW1). We will refer to the 19.3–18.7 ka B.P. warm event as Arabian Sea warm event II (ASW2). The SST values before and between these warm events are highly variable (~2°C); however, this variability is not mirrored in the δ^{18}O record. We focus on the concomitant δ^{18}O and SST events as they are more robust. After ASW1 the variability in the record is reduced to ~1°C, with an average of 23.5°C. The higher δ^{18}O interval at 14 ka B.P. has no (cold) counterpart in the SST

record. An abrupt rise in average SST of 0.7°C takes place at 12.9 ka B.P., which is within the period of rising $\delta^{18}O$ seen in the oxygen records.

5. Discussion

5.1. SST Records of Core NIOP929 in a Regional Context

[18] To evaluate the regional implications of the features in the Mg/Ca-derived SST record of core NIOP929 within the Arabian Sea the results are compared to SST records from core 93KL from the Pakistani margin, core 74KL located off Oman, ODP Hole 723A off Oman (18°05′10″N, 57°61′E, water depth 808 m) [*Naidu and Malmgren*, 2005], and core MD77194 off the tip of India (10°28′N, 75°14′E, water depth 1222 m) [*Cayre and Bard*, 1999; *Duplessy et al.*, 1981; *Sonzogni et al.*, 1998]. The SST records of these cores are based on different proxies than Mg/Ca, which is not ideal for comparison; other Mg/Ca SST records, however, are not available to date. In our comparison we use both annual average and seasonal SSTs. For core NIOP929 we give two proxy records that represent annual average SST: $U^{k'}_{37}$ SST and Mg/Ca SST of *G. ruber*. $U^{k'}_{37}$ is generally assumed to be an annual average SST proxy [*Bijma et al.*, 2001; *Budziak et al.*, 2000; *Herbert*, 2001; *Herbert et al.*, 1998; *Nürnberg et al.*, 2000; *Sachs et al.*, 2000; *Sonzogni et al.*, 1997a, 1997b; *Volkman*, 2000], and with roughly equal fluxes of *G. ruber* calcifying in summer and winter in the Arabian Sea [*Conan and Brummer*, 2000; *Curry et al.*, 1992] the Mg/Ca SST proxy can also be considered an annual average SST proxy. The 74KL seasonal SST records (summer and winter SST) are based on a transfer function using planktonic foraminiferal assemblages [*Schulz*, 1995]. Various SST records exist for core MD77194: a $U^{k'}{}_{37}$-based SST record [*Sonzogni et al.*, 1998] and a modern analogue technique based summer/winter SST record [*Cayre and Bard*, 1999]. The SST records (summer and winter) of core 723A are based on artificial neural network processing of foraminiferal assemblages.

[19] The Arabian Sea SST records, shown in Figure 7, show large variability; this could be partly due to the fact that the records are based on different proxies. The amplitude of the possible differences between various methods is illustrated in the SST records of cores NIOP929 and MD77194, which both combine $U^{k'}_{37}$ paleothermometry and an additional method. Partly, the discrepancies could point to markedly different SST evolutions through the Arabian Sea basin. The records are taken from widely varying monsoon provinces, and it is expected that this has resulted in very different local overprinting of the regional SST pattern. There are some similarities, however: The glacial-interglacial SST contrast in all shown records is 2°–3°C, and most of the records shown in Figure 7 place the late glacial initial warming in the Arabian Sea at ~19 ka B.P. In core NIOP929 the onset of deglacial warming could be placed at two events in the Mg/Ca SST record. A conservative approach would place the onset at 17 ka B.P., the base of ASW1, since at this level a temperature increase initiates persistent change toward Holocene temperatures. However, the temperature rise at 19 ka B.P., at the base of ASW2, can also be seen as the onset of deglacial warming. Average SST before this increase is lower than in the period between the ASW1 and ASW2. The period predating ASW2 covered by the record is very short, and its average SST is of limited significance. We therefore cannot conclusively assign a date to the onset of the deglacial warming in core NIOP929; the most conservative estimate, however, is 17 ka B.P. This is contemporaneous with the North Atlantic cold period associated with Heinrich event 1 [*Bond et al.*, 1993; *Heinrich*, 1988], which, by different authors, is placed between 18.1 and 14.6 ka B.P. [*Elliot et al.*, 1998; *Grousset et al.*, 2001; *Vidal et al.*, 1997; *Voelker et al.*, 2000]. Hole 723A differs with regard to the early deglacial warming. Whereas the summer SSTs at this site also show an early warming, the winter SST rise occurred around 14 ka B.P. This finding implies that the seasonal aspect of temperature change in the Arabian Sea is crucial in order to be able to fully assess the processes controlling climate change in the region. In Hole 723A, warm winter SSTs are approximately synchronous with ASW1 and ASW2, which corroborates the regional extent of these warm events. This was already indicated by the appearance of comparable low $\delta^{18}O$ events in the records of Figure 6.

[20] In the SST records of cores MD77194 and 74KL, comparable warm events are not seen; the former is located far from the other cores and may well lie outside the regional extent of the event. This is also possible for the latter, although its proximity to core NIOP929 increases the likelihood of an explanation for the difference between the proxies used.

[21] The maximum Mg/Ca SSTs in the period 13–10 ka B.P. in core NIOP929 are corroborated by the $U^{k'}_{37}$ SSTs, which show a similar maximum. The SST records from the other cores, however, show either constant or lower SSTs in this period, indicating that this warm phase as seen in core NIOP929 is most likely a local phenomenon, although it may also depend on the proxy used. The common early onset and amplitude of the glacial-interglacial temperature rise in all records shown indicates that in these aspects the (semi)global climate evolution dominates Arabian Sea SST.

5.2. Rapid SST Changes in the Arabian Sea

[22] The SST evolution of the Arabian Sea can be seen as interplay of monsoon influences and regional hydrography. By using the $\delta^{18}O$ and Mg/Ca SST records of core NIOP929 and previously published records we try to unravel this evolution. The $\delta^{18}O$ and Mg/Ca SST records of core NIOP929 register three major warm(ing) events. These are the warm pulses ASW1 and ASW2, found in both $\delta^{18}O$ and Mg/Ca SST, and the warming at 12.9 ka B.P., found only in the Mg/Ca SST record.

[23] There are a few potential scenarios that could explain the observed rapid temperature changes in the Arabian Sea. The first scenario invokes a variation in the monsoon-induced upwelling. During the last glacial the SW monsoon, and therefore upwelling, was not entirely terminated [*Anderson and Prell*, 1993; *Ivanova*, 1999; *Jung et al.*, 2002]. Consequently, variations in strength of the summer SW monsoon could have led to temperature variations,

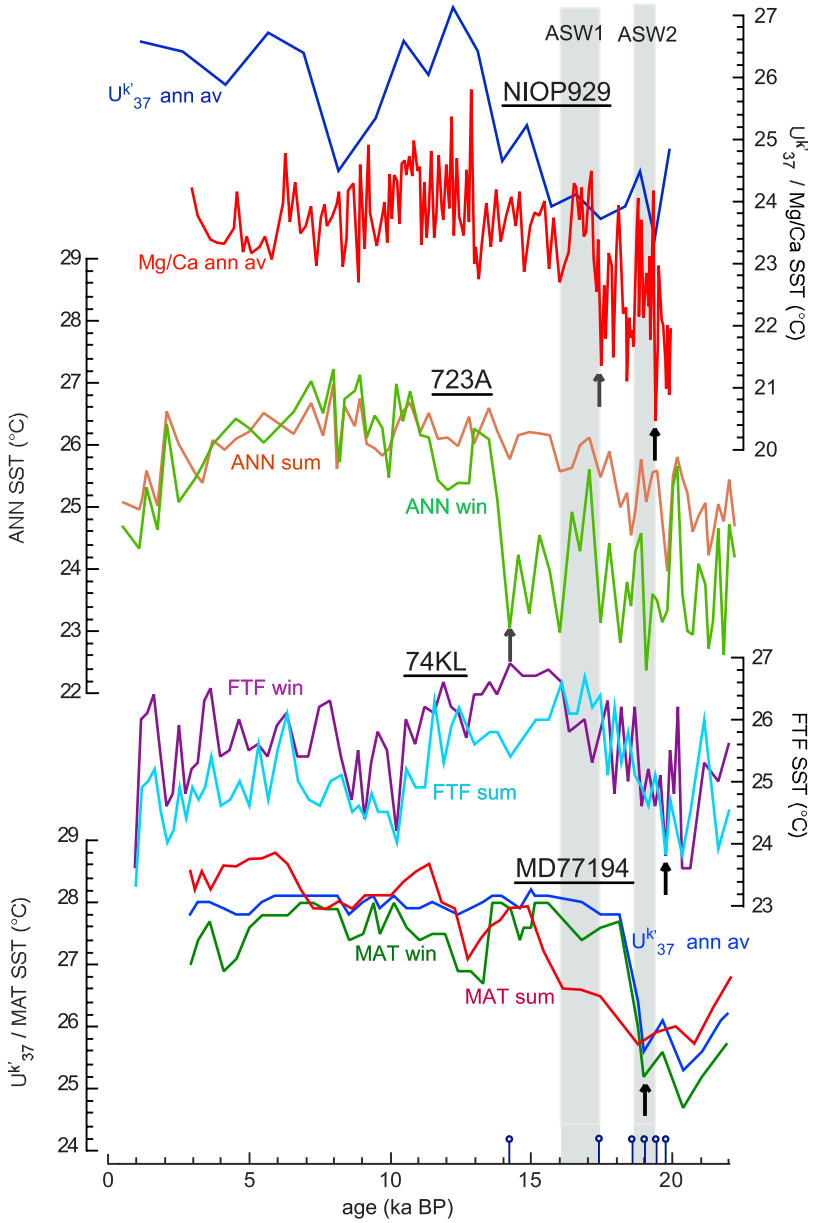

Figure 7. (Seasonal) SST comparison of core NIOP929 [*Rostek et al.*, 1997; this study], core 74KL [*Schulz*, 1995], Hole 723A [*Naidu and Malmgren*, 2005], and core MD77194 [*Cayre and Bard*, 1999]. The proxy indicated on the plot was used to make these comparisons. The $U^{k'}_{37}$ SST of core MD77194 was calculated using the equation of *Sonzogni et al.* [1997a]. The grey vertical bars highlight the warm pulses ASW1 and ASW2 in the core NIOP929 record and the approximate period of the Younger Dryas. Notice that the warm events observed in the core NIOP929 record are present in the Hole 723A record as well; it is most conspicuous in the winter SST. The vertical arrows and blue pins on the horizontal axis denote the onset of deglacial warming in all records and their projection on the time axis, respectively. Sum, summer; win, winter; ann av, annual average.

recorded both during glacial and interglacial periods. An increase in temperature of the upwelled water, due to a different (possibly shallower) provenance, or a somehow enhanced incorporation of warm ambient surface water in the upwelling cells could also have caused temperature shifts.

[24] Palaeoproductivity records document when upwelling intensity, and thus SW monsoon strength, may have changed, so we plotted our SST record against the organic carbon content (percent TOC) of core NIOP929 and two other Arabian Sea cores: SO93-111KL (23°05′80″N, 66°29′02″E, water depth 775 m) and SO93-136KL (23°07′34″N, 66°29′83″E, water depth 568 m) [*Schulz et*

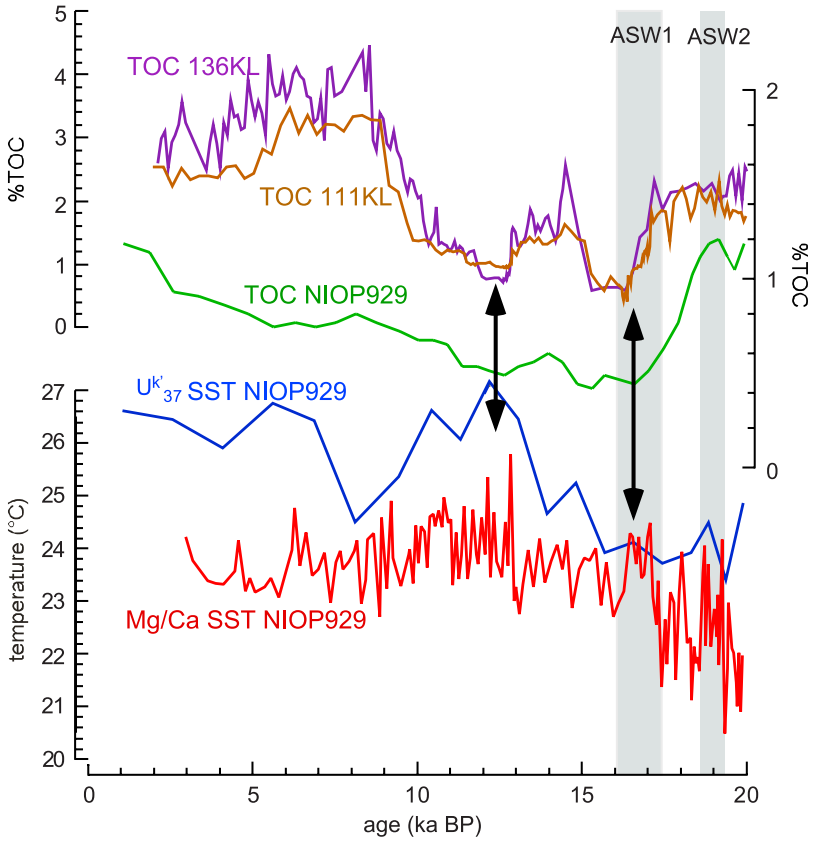

Figure 8. NIOP929 SST records compared with the percent TOC records of NIOP929 [*Ivanova*, 1999], 111KL, and 136KL [*Schulz et al.*, 1998]. For increased visibility the percent TOC record of core NIOP929 was plotted on a different vertical scale. Notice that the periods of low organic content tend to coincide with the periods of high SST. The grey bars indicate ASW1 and ASW2.

al., 1998] (Figure 8). This exercise provides some clues concerning upwelling variability resulting in SST changes. The same millennial-scale productivity patterns are observed in the northern and western Arabian Sea, with lowest values around 16 and 12 ka B.P. In these low-productivity periods, SSTs are relatively high, suggesting a negative correlation. These patterns could be explained by upwelling variability at the millennial scale and assuming NE monsoon cooling played only a minor role. The Hole 723A seasonal SST record supports reduced upwelling as an explanation for ASW2 as it displays a warm summer SST event synchronous with ASW2. Hole 723A is also located in an upwelling area, and reduced upwelling would logically result in higher summer SSTs at this location. This upwelling scenario is not ubiquitously applicable as an explanation for SST changes, however; ASW2 is concomitant with a period of high TOC content and thus high productivity. Another argument against upwelling variability as an explanation for ASW1 and ASW2 concerns the similarity in the δ^{18}O records of sediment cores NIOP929, 74KL, and 93KL. Figure 6 shows that the δ^{18}O minima at the times of ASW1 and ASW2 are recorded in all three cores, although core 93KL is located outside the main upwelling areas; hence the δ^{18}O variations at this site cannot be explained by SW monsoon-induced changes in the surface ocean. Additionally, *Naidu and Malmgren* [1995] and *Overpeck et al.* [1996] mention a SW monsoon increase, and not a decrease, around 13 ka B.P. Altogether, there are arguments both for and against reduced upwelling as an explanation for all three individual warmings.

[25] Another scenario concerns fluctuations in NE monsoon. In glacial times the NE monsoon was invigorated and therefore probably exerted a larger influence on Arabian Sea SST than during interglacial time periods [*Duplessy*, 1982; *Fontugne and Duplessy*, 1986; *Prell and Campo*, 1986]. Assuming a stronger impact of the glacial NE monsoon on the sea surface temperature history on a basin-scale, NE monsoon variability during the deglaciation would have caused SST changes of higher amplitude than now observed in the western Arabian Sea. Winter SST in Hole 723A displays a warming during ASW1, which supports a causal relationship between at least ASW1 and the NE monsoon. An argument against NE monsoon variability causing ASW1 and ASW2 is equivalent to the one that argues against SW monsoon variability: the comparable magnitude of the events in cores from very different (monsoonal) provenances. Another argument against reduced NE monsoon as the cause for ASW1 is that this warming is

contemporaneous with Heinrich event 1. Several authors [*de Garidel-Thoron et al.*, 2001; *Ivanova*, 1999; *Schulz et al.*, 2002] have argued that during this period the NE monsoon was invigorated, which would result in surface cooling; yet the opposite is found. Altogether, it is possible that NE monsoon variability did contribute to the warmings observed in the NIOP929 records; it is, however, not likely to have been a major factor.

[26] A third possibility is a change in water/heat advection in the Indian Ocean. The South Equatorial Current flows westward toward Madagascar [*Schott et al.*, 2002], where it splits into a northern and southern branch. The northern branch, the Northeast Madagascar Current, merges into the East African Coast Current, bringing warm water into the Arabian Sea. An increase in this influx, possibly related to invigorated trade wind strength, may have caused the SST rises seen in the core NIOP929 records.

[27] A strengthening of the trade winds in the last glacial, as inferred by *Bush and Philander* [1998], would increase the influx of warm water toward the Arabian Sea [*Jung et al.*, 2004], which could explain rapid SST variations. As trade winds affect both the Indo-Pacific Warm Pool (IPWP) and the Arabian Sea, assuming a prominent role for this phenomenon in determining SST would indirectly imply some similarity in SST evolution of both basins. Interestingly, IPWP SSTs, just like core NIOP929 SSTs, started to rise early from glacial minimum levels: at ~20 ka B.P. [*Rosenthal et al.*, 2003] and ~19 ka B.P. [*Visser et al.*, 2003]. All mentioned records reach interglacial SST levels around 11 ka B.P. *Kim and Schneider* [2003] indicate strong trade winds in the late glacial period, which would corroborate a trade wind related cause for ASW1 and ASW2. *Koutavas et al.* [2002], however, suggest the opposite. As none of the other Arabian Sea SST records (Figure 7) show a warming in this period, a large-scale phenomenon such as increased warm water advection is a less likely explanation for this 13 ka B.P. warming; however, the discrepancy between core NIOP929 and the other cores could also be due to the use of different proxies.

[28] Summarizing, we cannot conclusively assign a specific scenario to any of the warmings we discussed. A single Mg/Ca-based SST record is insufficient for unraveling the complex SST history of the Arabian Sea, in which most likely all the mentioned scenarios for rapid SST change operate simultaneously.

6. Conclusions

[29] In the present study we present new high-resolution $\delta^{18}O$ and Mg/Ca records from core NIOP929 from the Arabian Sea off Oman, leading to four main conclusions.

[30] 1. The NIOP929 SST record shows an early onset of the temperature rise associated with termination I, which could be placed at either 19 or 17 ka B.P. This early warming is in line with several other Arabian Sea SST records that show an onset at ~19 ka B.P.

[31] 2. The $\delta^{18}O$ record depicts two short-term minimum spikes at 17 and 19 ka B.P. On the basis of a comparison with previously published time series on a SW-NE transect across the Arabian Sea these events may be a basin-wide phenomenon. The $\delta^{18}O$ minima are mirrored by maxima in the Mg/Ca temperature record. We refer to these warm periods as Arabian Sea warm events (ASW) 1 and 2, respectively. A combined assessment of $\delta^{18}O$ and Mg/Ca temperatures suggests that the most likely cause for these warmings is a combination of monsoon variations and fluctuations in trade wind induced advection of equatorial warm water.

[32] 3. ASW1 is, within limitations of the age model, synchronous with the (cold) Northern Hemisphere Heinrich event 1.

[33] 4. The core NIOP929 temperature record implies a stepwise warming of roughly 2°C during the glacial-Holocene transition. Roughly 75% of this increase is reached before 15 ka B.P. These findings are corroborated by similar values in other Arabian Sea SST records.

[34] **Acknowledgments.** The Mg/Ca measurements were made possible by the EU CESOP program. The manuscript benefited greatly from the constructive comments of Steven Clemens and an anonymous reviewer.

References

Alley, R. B., E. J. Brook, and S. Anandakrishnan (2002), A northern lead in the orbital band: North-south phasing of ice-age events, *Quat. Sci. Rev.*, *21*, 431–441.

Altabet, M. A., R. Francois, D. W. Murray, and W. L. Prell (1995), Climate-related variations in denitrification in the Arabian Sea from sediment $^{15}N/^{14}N$ ratios, *Nature*, *373*, 506–509.

Anand, P., H. Elderfield, and M. H. Conte (2003), Calibration of Mg/Ca thermometry in planktonic foraminifera from a sediment trap time series, *Paleoceanography*, *18*(2), 1050, doi:10.1029/2002PA000846.

Anderson, D. M., and W. L. Prell (1993), A 300 kyr record of upwelling off Oman during the late Quaternary: Evidence of the Asian southwest monsoon, *Paleoceanography*, *8*, 193–208.

Bard, E., F. Rostek, and C. Sonzogni (1997), Interhemispheric synchrony of the last deglaciation inferred from alkenone paleothermometry, *Nature*, *385*, 707–710.

Barker, S., and H. Elderfield (2002), Foraminiferal calcification response to glacial-interglacial changes in atmospheric CO_2, *Science*, *297*, 833–836.

Barker, S., M. Greaves, and H. Elderfield (2003), A study of cleaning procedures used for foraminiferal Mg/Ca paleothermometry, *Geochem. Geophys. Geosyst.*, *4*(9), 8407, doi:10.1029/2003GC000559.

Benn, D. I., and L. A. Owen (1998), The role of the Indian summer monsoon and the midlatitude westerlies in Himalayan glaciation: Review and speculative discussion, *J. Geol. Soc.*, *155*, 353–363.

Bigg, G. R., and D. Jiang (1993), Modeling the late Quaternary Indian Ocean circulation, *Paleoceanography*, *8*, 23–46.

Bijma, J., M. Altabet, M. Conte, H. Kinkel, G. J. M. Versteegh, J. K. Volkman, S. G. Wakeham, and P. P. Weaver (2001), Primary signal: Ecological and environmental factors—Report from Working Group 2, *Geochem. Geophys. Geosyst.*, *2*(1), doi:10.1029/2000GC000051.

Bijma, J., B. Hönisch, and R. E. Zeebe (2002), Impact of the ocean carbonate chemistry on living foraminiferal shell weight: Comment on "Carbonate ion concentration in glacial-age deep waters of the Caribbean Sea" by W. S. Broecker and E. Clark, *Geochem. Geophys. Geosyst.*, *3*(11), 1064, doi:10.1029/2002GC000388.

Blunier, T., and E. J. Brook (2001), Timing of millennial-scale climate change in Antarctica and Greenland during the last glacial period, *Science*, *291*, 109–112.

Blunier, T., et al. (1998), Asynchrony of Antarctic and Greenland climate change during the last glacial period, *Nature*, *394*, 739–743.

Bond, G., W. Broecker, S. Johnsen, J. McManus, L. Labeyrie, J. Jouzel, and G. Bonani (1993), Correlations between climate records from North Atlantic sediments and Greenland ice, *Nature*, *365*, 143–147.

Brock, J. C., C. R. McClain, D. M. Anderson, W. L. Prell, and W. W. Hay (1992), Southwest monsoon circulation and environments of recent planktonic foraminifera in the northwestern Arabian sea, *Paleoceanography*, *7*, 799–813.

Broecker, W. S. (1998), Paleocean circulation during the last deglaciation: A bipolar seesaw?, *Paleoceanography*, *13*, 119–121.

Broecker, W. S., and E. Clark (2001a), $CaCO_3$ size distribution: A paleocarbonate ion proxy?, *Paleoceanography*, *16*, 596–604.

Broecker, W., and E. Clark (2001b), An evaluation of Lohmann's foraminifera weight dissolution index, *Paleoceanography*, *16*, 531–534.

Brown, S. J., and H. Elderfield (1996), Variations in Mg/Ca and Sr/Ca ratios of planktonic foraminifera caused by postdepositional dissolution: Evidence of shallow Mg-dependent dissolution, *Paleoceanography*, *11*, 543–552.

Budziak, D., R. R. Schneider, F. Rostek, P. J. Müller, E. Bard, and G. Wefer (2000), Late Quaternary insolation forcing on total organic carbon and C_{37} alkenone variations in the Arabian Sea, *Paleoceanography*, *15*, 307–321.

Bush, A. B. G., and S. G. H. Philander (1998), The role of ocean-atmosphere interactions in tropical cooling during the Last Glacial Maximum, *Science*, *279*, 1341–1344.

Cayre, O., and E. Bard (1999), Planktonic foraminiferal and alkenone records of the last deglaciation from the eastern Arabian Sea, *Quat. Res.*, *52*, 337–342.

Conan, S. M.-H., and G.-J. A. Brummer (2000), Fluxes of planktic foraminifera in response to monsoonal upwelling on the Somalia Basin margin, *Deep Sea Res., Part II*, *47*, 2207–2227.

Conan, S. M.-H., E. M. Ivanova, and G.-J. A. Brummer (2002), Quantifying carbonate dissolution and calibration of foraminiferal dissolution indices in the Somali Basin, *Mar. Geol.*, *182*, 325–349.

Curry, W. B., D. R. Ostermann, M. V. S. Guptha, and V. Ittekkot (1992), Foraminiferal production and monsoonal upwelling in the Arabian Sea: Evidence from sediment traps, in *Upwelling Systems: Evolution Since the Miocene*, edited by C. P. Summerhayes et al., *Geol. Soc. Spec. Publ.*, *64*, 93–106.

de Garidel-Thoron, T., L. Beaufort, B. K. Linsley, and S. Dannenmann (2001), Millennial-scale dynamics of the east Asian winter monsoon during the last 200000 years, *Paleoceanography*, *16*, 491–502.

de Villiers, S. (2003), A 425 kyr record of foraminiferal shell weight variability in the western equatorial Pacific, *Paleoceanography*, *18*(4), 1080, doi:10.1029/2002PA000801.

de Villiers, S., M. Greaves, and H. Elderfield (2002), An intensity ratio calibration method for the accurate determination of Mg/Ca and Sr/Ca of marine carbonates by ICP-AES, *Geochem. Geophys. Geosyst.*, *3*(1), 1001, doi:10.1029/2001GC000169.

Duplessy, J. C. (1982), Glacial to interglacial contrasts in the northern Indian Ocean, *Nature*, *295*, 494–498.

Duplessy, J. C., A. W. H. Be, and P. L. Blanc (1981), Oxygen and carbon isotopic composition and biogeographic distribution of planktonic foraminifera in the Indian Ocean, *Palaeogeogr. Palaeoclimatol. Palaeoecol.*, *33*, 9–46.

Elderfield, H., and G. Ganssen (2000), Past temperatures and $\delta^{18}O$ of surface ocean waters inferred from foraminiferal Mg/Ca ratios, *Nature*, *405*, 442–445.

Elliot, M., L. Labeyrie, G. Bond, E. Cortijo, J.-L. Turon, N. Tisnerat, and J.-C. Duplessy (1998), Millennial-scale iceberg discharges in the Irminger Basin during the last glacial period: Relationship with the Heinrich events and environmental settings, *Paleoceanography*, *13*, 433–446.

Emeis, K.-C., D. M. Anderson, H. Doose, D. Kroon, and D. Schultz-Bull (1995), Sea surface temperatures and the history of monsoon upwelling in the northwest Arabian Sea during the last 500000 years, *Quat. Res.*, 355–361.

Fontugne, M. R., and J. C. Duplessy (1986), Variations of the monsoon regime during the upper Quaternary: Evidence from carbon isotopic record of organic matter in north Indian Ocean sediment cores, *Palaeogeogr. Palaeoclimatol. Palaeoecol.*, *56*, 69–88.

Grousset, F. E., E. Cortijo, S. Huon, L. Hervé, T. Richter, D. Burdloff, J. Duprat, and O. Weber (2001), Zooming in on Heinrich layers, *Paleoceanography*, *16*, 240–259.

Heinrich, H. (1988), Origin and consequences of cyclic ice rafting in the northeast Atlantic Ocean during the past 130000 years, *Quat. Res.*, *29*, 143–152.

Herbert, T. D. (2001), Review of alkenone calibrations (culture, water column, and sediments), *Geochem. Geophys. Geosyst.*, *2*(2), doi:10.1029/2000GC000055.

Herbert, T. D., J. D. Schuffert, D. Thomas, C. Lange, A. Weinheimer, A. Peleo-Alampay, and J.-C. Herguera (1998), Depth and seasonality of alkenone production along the California margin inferred from a core top transect, *Paleoceanography*, *13*, 236–271.

Ivanochko, T. S., R. S. Ganeshram, G.-J. A. Brummer, G. Ganssen, S. J. A. Jung, S. G. Moreton, and D. Kroon (2005), Variations in tropical convection as an amplifier of global climate change at the millennial scale, *Earth Planet. Sci. Lett.*, *235*, 302–314.

Ivanova, E. (1999), Late quaternary monsoon history and paleoproductivity of the western Arabian Sea, Ph.D. dissertation, Free Univ., Amsterdam.

Jung, S. J.A., E. Ivanova, G. J. Reichart, G. R. Davies, G. M. Ganssen, D. Kroon, J. E. van Hinte (2002), Centennial-millennial-scale monsoon variations off Sofmalia over the last 35 ka, in *The Tectonic and Climatic Evolution of the Arabian Sea Region*, edited by P. D. Clift et al., *Geol. Soc. Spec. Publ.*, 195, 341–352.

Jung, S. J. A., G. R. Davies, G. M. Ganssen, and D. Kroon (2004), Synchronous Holocene sea surface temperature and rainfall variations in the Asian monsoon system, *Quat. Sci. Rev.*, *23*, 2207–2218.

Kim, J.-H., and R. R. Schneider (2003), Low-latitude control of interhemispheric sea surface temperature contrast in the tropical Atlantic over the past 21 k years: The possible role of SE trade winds, *Clim. Dyn.*, *21*, 337–347.

Koutavas, A., J. Lynch-Stieglitz, T. M. Marchitto Jr., and J. P. Sachs (2002), El Nino-like pattern in ice age tropical Pacific sea surface temperature, *Science*, *297*, 226–230.

Leuschner, D. C., and F. Sirocko (2000), The low-latitude monsoon climate during Dansgaard-Oeschger cycles and Heinrich events, *Quat. Sci. Rev.*, *19*, 243–254.

Lohmann, G. P. (1995), A model for variation in the chemistry of planktonic foraminifera due to secondary calcification and selective dissolution, *Paleoceanography*, *10*, 445–457.

Mix, A. C., E. Bard, and R. Schneider (2001), Environmental processes of the ice age: Land, oceans, glaciers (EPILOG), *Quat. Sci. Rev.*, *20*, 627–657.

Naidu, P. D., and B. A. Malmgren (1995), A 2200 years periodicity in the Asian monsoon system, *Geophys. Res. Lett.*, *22*, 2361–2364.

Naidu, P. D., and B. A. Malmgren (2005), Seasonal sea surface temperature contrast between the Holocene and last glacial period in the western Arabian Sea (Ocean Drilling Project Site 723A): Modulated by monsoon upwelling, *Paleoceanography*, *20*, PA1004, doi:10.1029/2004PA001078.

Nürnberg, D., A. Müller, and R. R. Schneider (2000), Paleo-sea surface temperature calculations in the equatorial east Atlantic from Mg/Ca ratios in planktic foraminifera: A comparison to sea surface temperature estimates from $U^{K'}_{37}$, oxygen isotopes, and foraminiferal transfer function, *Paleoceanography*, *15*, 124–134.

Overpeck, J., D. Anderson, S. Trumbore, and W. Prell (1996), The southwest Indian monsoon over the last 18000 years, *Clim. Dyn.*, *12*, 213–225.

Prell, W. L., and E. V. Campo (1986), Coherent response of Arabian Sea upwelling and pollen transport to late Quaternary monsoonal winds, *Nature*, *323*, 526–528.

Prell, W. L., and W. B. Curry (1981), Faunal and isotopic indices of monsoonal upwelling, western Arabian Sea, *Oceanol. Acta*, *4*, 91–98.

Prell, W. L., D. W. Murray, S. C. Clemens, and D. M. Anderson (1992), Evolution and variability of the Indian Ocean summer monsoon: Evidence from the western Arabian Sea drilling programme, in *Synthesis of Results From Scientific Drilling in the Indian Ocean*, *Geophys. Monogr. Ser.*, vol. 70, edited by R. A. Duncan et al., pp. 447-469, AGU, Washington, D. C.

Reichart, G. J., L. J. Lourens, and W. J. Zachariasse (1998), Temporal variability in the northern Arabian Sea oxygen minimum zone (OMZ) during the last 225000 years, *Paleoceanography*, *13*, 607–621.

Rixen, T., B. Haake, V. Ittekkot, M. V. S. Gunptha, R. R. Nair, and P. Schlüssel (1996), Coupling between SW monsoon-related surface and deep ocean processes as discerned from continuous particle flux measurements and correlated satellite data, *J. Geophys. Res.*, *101*, 28,569–28,582.

Rosenthal, Y., and G. P. Lohmann (2002), Accurate estimation of sea surface temperatures using dissolution-corrected calibrations for Mg/Ca thermometry, *Paleoceanography*, *17*(3), 1044, doi:10.1029/2001PA000749.

Rosenthal, Y., G. P. Lohmann, K. C. Lohmann, and R. M. Sherrell (2000), Incorporation and preservation of Mg in *Globigerinoides sacculifer*: Implications for reconstructing the temperature and 18O/16O of seawater, *Paleoceanography*, *15*, 135–145.

Rosenthal, Y., D. W. Oppo, and B. K. Linsley (2003), The amplitude and phasing of climate change during the last deglaciation in the Sulu Sea, western equatorial Pacific, *Geophys. Res. Lett.*, *30*(8), 1428, doi:10.1029/2002GL016612.

Rostek, F., E. Bard, L. Beaufort, C. Sonzogni, and G. Ganssen (1997), Sea surface tempera-

ture and productivity records for the past 240 kyr in the Arabian Sea, *Deep Sea Res., Part II*, *44*, 1461–1480.

Sachs, J. P., R. R. Schneider, T. I. Eglinton, K. H. Freeman, G. Ganssen, J. F. McManus, and D. W. Oppo (2000), Alkenones as paleoceanographic proxies, *Geochem. Geophys. Geosyst.*, *1*(11), doi:10.1029/2000GC000059.

Schott, F. A., M. Dengler, and R. Schoenefeldt (2002), The shallow overturning circulation of the Indian Ocean, *Prog. Oceanogr.*, *53*, 57–103.

Schulte, S., and P. J. Müller (2001), Variations of sea surface temperature and primary productivity during Heinrich and Dansgaard-Oeschger events in the northeastern Arabian Sea, *Geo. Mar. Lett.*, *21*, 168–175.

Schulz, H. (1995), Meeresoberflächentemperaturen vor 10000 Jahren—Auswirkungen des frühholozänen Insolationsmaximums, *Ber. 73*, 156 pp., Geol.-Paläontol. Inst., Univ. Kiel, Kiel, Germany.

Schulz, H., U. von Rad, and H. Erlenkeuser (1998), Correlation between Arabian Sea and Greenland climate oscillations of the past 110000 years, *Nature*, *393*, 54–57.

Schulz, H., von U. Rad, V. Ittekkot (2002), Planktic foraminifera, particle flux and oceanic productivity off Pakistan, NE Arabian Sea: Modern analogues and application to the palaeoclimatic record, in *The Tectonic and Climatic Evolution of the Arabian Sea Region*, edited by P. D. Clift et al., *Geol. Soc. Spec. Publ.*, 195, 499–516.

Shetye, S. R., A. D. Gouveia, and S. S. Shenoi (1994), Circulation and water masses of the Arabian Sea, *Proc. Indian Acad. Sci. Earth Planet. Sci.*, *103*, 107–123.

Sirocko, F., M. Sarnthein, H. Erlenkeuser, H. Lange, M. Arnold, and J. C. Duplessy (1993), Century-scale events in monsoonal climate over the past 24000 years, *Nature*, *364*, 322–324.

Sonzogni, C., E. Bard, F. Rostek, D. Dollfus, A. Rosell-Mele, and G. Eglington (1997a), Temperature and salinity effects on alkenone ratios measured in surface sediments from the Indian Ocean, *Quat. Res.*, *47*, 344–355.

Sonzogni, C., E. Bard, F. Rostek, R. Lafont, A. Rosell-Mele, and G. Eglinton (1997b), Core-top calibration of the alkenone index versus sea surface temperature in the Indian Ocean, *Deep Sea Res., Part II*, *44*, 1445–1460.

Sonzogni, C., E. Bard, and F. Rostek (1998), Tropical sea surface temperatures during the last glacial period: A view based on alkenones in Indian Ocean sediments, *Quat. Sci. Rev.*, *17*, 1185–1201.

Southon, J., M. Kashgarian, M. Fontugne, B. Metivier, and W. W.-S. Yim (2002), Marine reservoir corrections for the Indian Ocean and Southeast Asia, *Radiocarbon*, *44*, 167–180.

Staubwasser, M., F. Sirocko, P. M. Grootes, and H. Erlenkeuser (2002), South Asian monsoon climate change and radiocarbon in the Arabian Sea during early and middle Holocene, *Paleoceanography*, *17*(4), 1063, doi:10.1029/2000PA000608.

Stuiver, M., and P. Reimer (1993), Extended ^{14}C data base and revised CALIB 3.0 ^{14}C age calibration program, *Radiocarbon*, *35*, 215–230.

ten Haven, H. L., and D. Kroon (1991), Late Pleistocene sea surface water temperature variations off Oman as revealed by the distribution of long-chain alkenones, *Proc. Ocean Drill. Program Sci. Results.*, *117*, 445–452.

van Hinte, J. E., T. C. E. van Weering, and S. R. Troelstra (1995), *Tracing a Seasonal Upwelling*, *Rep. 4*, 146 pp., Natl. Mus. Nat. Hist., Leiden, Netherlands.

Vidal, L., L. Labeyrie, E. Cortijo, M. Arnold, J. C. Duplessy, E. Michel, S. Becque, and T. C. E. van Weering (1997), Evidence for changes in the North Atlantic Deep Water linked to meltwater surges during the Heinrich events, *Earth Planet. Sci. Lett.*, *146*, 13–27.

Visser, K., R. Thunell, and L. Stott (2003), Magnitude and timing of temperature change in the Indo-Pacific Warm Pool during deglaciation, *Nature*, *421*, 152–154.

Voelker, A. H. L., P. M. Grootes, M.-J. Nadeau, and M. Sarnthein (2000), Radiocarbon levels in the Iceland Sea from 25–53 kyr and their link to the Earth's magnetic field intensity, *Radiocarbon*, *42*, 437–452.

Volkman, J. K. (2000), Ecological and environmental factors affecting alkenone distributions in seawater and sediments, *Geochem. Geophys. Geosyst.*, *1*(9), doi:10.1029/2000GC000061.

von Rad, U., H. Schulz, V. Riech, M. de Dulk, U. Berner, and F. Sirocko (1999), Multiple monsoon-controlled breakdown of oxygen-minimum conditions during the past 30000 years documented in laminated sediments off Pakistan, *Palaeogeogr. Palaeoclimatol. Palaeoecol.*, *152*, 129–161.

Webster, P. J., V. O. Magaña, T. N. Palmer, J. Shukla, R. A. Tomas, M. Yanai, and T. Yasunari (1998), Monsoons: Processes, predictability, and the prospects for prediction, *J. Geophys. Res.*, *103*, 14,451–14,510.

H. Elderfield and M. J. Greaves, Department of Earth Sciences, University of Cambridge, Downing Street, Cambridge CB2 3EQ, UK.

S. J. A. Jung, D. Kroon, and M. H. Saher, Institute of Earth Sciences, Vrije Universiteit Amsterdam, De Boelelaan 1085, 1081HV Amsterdam, Netherlands. (margot.saher@falw.vu.nl)